Porosity in chalk – roles of elastic strain and plastic strain

Fabricius, Ida Lykke

Published in:
Sedimentology

Link to article, DOI:
10.1111/sed.12750

Publication date:
2020

Document Version
Peer reviewed version

PROF. IDA LYKKE FABRICIUS (Orcid ID : 0000-0002-5292-1384)

Article type : Original Manuscript

Porosity in chalk – roles of elastic strain and plastic strain

IDA LYKKE FABRICIUS*

**Department of Civil Engineering, Technical University of Denmark, DTU Brovej 118, DK-2800 Kongens Lyngby, Denmark (E-mail: ilfa@byg.dtu.dk)*

Associate Editor – John Reijmer

Short Title – Porosity in chalk

ABSTRACT

Chalks originate as Cretaceous to Recent pelagic or hemipelagic calcareous ooze, which indurate via burial diagenesis to chalk and limestone. Because they accumulate in pelagic settings with high environmental continuity, chalks may form thick formations and even groups. For this reason and because chalks have a simple mineralogy (low magnesium calcite, silica and clays), they are ideal for the study of diagenetic processes including the depth-related decrease of porosity. It is the aim of this study to illustrate how the evaluation of *in situ* elastic strain can help in understanding these processes including the interplay between stress-controlled diagenetic processes and processes furthered by thermal energy. Petrophysical core and well data can be used for analyses of how porosity reduction via pore collapse and pressure dissolution is related to *in situ* elastic strain. The data in question are:

depth, density of overburden, pore pressure, ultrasonic P-wave velocity and dry density/porosity. The analysis reveals that the transition from ooze to chalk is associated with high elastic strain and consequent pressure dissolution at calcite–particle contacts causing contact cementation. The transition from chalk to limestone is also associated with high elastic strain, especially at clay–calcite interphases causing development of stylolites via pressure dissolution, and consequent pore-filling cementation. Following each transformation the elastic strain drops rapidly. The observation of this diagenesis-related pattern in elastic strain of the sedimentary rock is novel and should not only be helpful in understanding the porosity development in sedimentary basins, but also add basic scientific insight.

Keywords Burial, diagenesis, elasticity, pore-collapse, pressure dissolution.

INTRODUCTION

Burial diagenesis involves compaction and induration caused by plastic deformation and pressure dissolution, and it can be discussed in terms of depth, where depth is, in reality, a proxy for stress and temperature. Temperature – quantified in terms of accumulated thermal energy – causes mineralogical transformations. Stress generates strain energy – quantified in terms of resulting elastic strain – and in this way causes volume reduction. Whereas stress is an ill-defined term that depends on reference area and material properties, elastic strain is well-defined, so the aim of this paper is to illustrate how quantifying the elastic strain can help in understanding stress-driven diagenetic processes, where chalk is used as an example. The compaction will be quantified in terms of porosity, and the induration will be quantified in terms of Biot's coefficient.

Chalks occur in massive formations on continents, continental shelves and on oceanic plateaus. On continents, chalks are typically of Late Cretaceous age as a reflection of high sea-level (e.g. Gale, 2000). On subsiding passive continental shelves, chalk deposition can have continued into the Cenozoic, as for example in the North Sea basin where early Palaeogene (Danian) chalks are found (e.g. van Buchem *et al*., 2017). On oceanic plateaus, chalk deposition can have prevailed from Early Cretaceous to present (e.g. Berger *et al*.,

1992). Chalks are pelagic or hemipelagic sedimentary rocks mainly composed of partly or fully recrystallized biogenic particles of chemically stable low Mg-calcite (Black, 1963). These biogenic particles include calcareous nannofossil crystal elements 0.2 to 1.0 μm in size, nannofossils of silt size, and microfossils of millimetre size (Figs 1 and 2; Håkansson *et al.*, 1974). The size of the nannofossils has been found to vary through geological time as a function of ocean chemistry (Bolton *et al.*, 2016). In some beds, chalk intraclasts prevail and in continental outcrops, fossil debris and macrofossils catch the eye (e.g. Hansen & Surlyk, 2014). Non-carbonate particles primarily include biogenic opal-A as well as diagenetic opal-CT and micro-quartz (Figs 3 and 4; Wise Jr & Kelts, 1972; Ehrmann, 1986; Hjuler & Fabricius, 2009; Madsen & Stemmerik, 2010). Remnants of opal-A can be found as partly or fully dissolved siliceous microfossils, which in thin section are visible as collapsed fossil remains or moulds (Fig. 3). Clay can be detrital and occur as lithoclasts (Fabricius *et al.*, 2007a), but kaolinite typically occur as pore-filling cement, in some cases associated with micro-quartz (Fig. 4). Minor amounts of siliciclastic silt, biogenic apatite and diagenetic pyrite, dolomite, barite/strontianite and zeolites can be found. According to the Dunham (1962) classification, most chalks would have mudstone texture, but Crabtree *et al.* (1996) introduced a modified Dunham classification, where the contrast in particle size classes rather than an absolute threshold among classes is emphasized, so that microfossils, intraclasts and fossil fragments will be counted as grains, nannofossils and crystalline elements as mud. Most chalks from North Sea petroleum reservoirs accordingly have a depositional texture which may be referred to as mudstone or wackestone (with more than 10% grain area in thin section; Fig. 1). Chalk with packstone texture only occurs sporadically (Fig. 1).

Whereas the particle size distribution in chalk thus can be rather complicated, most chalks have rather narrowly defined pore size distributions with only minor contributions from larger intra-fossil pores or small pores among silicates (Faÿ-Gomord *et al.*, 2016). It is a characteristic of chalk that the relatively large intra-fossil pores have little effect on permeability, because they are connected through the fine inter-particle pores (Fabricius *et al.*, 2007b), but that the fine pore space is well connected. As an example, polyester resin casts of 13 to 17% porosity chalk from Yorkshire indicate a high connectivity (14 to 17) among pores, a mean pore diameter of 3 to 5 μm, and a mean pore throat

diameter of 1 to 2 μm (Patsoules & Cripps, 1982). Even for this relatively low-porosity chalk, pore size is much larger than what would correspond to micropores in physical chemistry, where micropores have diameter of less than 2 nm as defined from gas adsorption (Rouquerol *et al.*, 1994). According to a reservoir geological definition, micropores have a size of *ca* 0.2 μm to *ca* 10 μm and are supposed to be bypassed during water flooding (Hasiuk *et al*., 2016). According to this alternative definition, chalk pore space is largely composed of micropores, although this again is ambiguous, because water flooding passes through these supposed micropores (e.g. Korsbech *et al.*, 2006).

A relation between depositional texture and porosity is rarely seen, but the degree of mixing of components determines the inter-particle porosity (Maliva & Dickson, 1992; Fabricius *et al*., 2007b; Meyer *et al.*, 2019; Saïag *et al.*, 2019). The resulting inter-particle porosity is high whenever only one grain size class is present, low when silica and/or clay prevail in the pore space of the carbonate mud. Where intrafossil porosity is open, it has little influence on porosity because the walls of fossil shells compensate by being relatively thick, but when the intra-fossil porosity is occluded by cement, the presence of microfossils will reduce porosity (Borre & Fabricius, 1998). A high porosity chalk would typically have high carbonate content and mudstone texture; a low porosity chalk could have packstone texture and a carbonate content of 75% (Fig. 1). Some intervals of high porosity chalk may have been redeposited via mass transport of the primary sediment (Kennedy, 1980; Hatton, 1986), and the presence of intraclasts indicates mass transport, but it does not indicate either high or low porosity (Fabricius *et al*., 2007b; Anderskouv & Surlyk, 2012). Some high porosity intervals of mudstone or grainstone can have a narrow range of grain size due to redeposition after transport by traction currents or due to winnowing of the primary sediment (Cooke *et al*., 2004; Bulls *et al*., 2017).

Although porosity in chalk can vary significantly due to textural variations, overall, porosity decreases with burial depth, and several workers have constructed porosity-depth curves for chalks (e.g. Scholle, 1977; Urmos *et al*., 1993; Mallon & Swarbrick, 2002), and some workers have noticed that the presence of hydrocarbons and overpressure in the pore space retards depth-related porosity decrease (e.g. D'Heur, 1984; Japsen, 1998).

The depth-related porosity reduction involves processes promoted by thermal energy as well as processes promoted by stress. Thermal energy is controlled by heat flow and rate of deposition/rate of subsidence and can be modelled in a well-defined way, as for example by Lopatins Time-Temperature-Index (TTI) concept (Lopatin, 1971; Waples, 1980). The TTI basically quantifies the total thermal energy a sediment or sedimentary rock has absorbed, by summing up the product of temperature and time spent in a sequence of temperature intervals.

Processes requiring thermal energy include recrystallization of calcite after sediment deposition, which takes place because calcite surfaces will either dissolve or develop overgrowth until stable rhombohedral faces are obtained (Neugebauer, 1974; Burns, 1975). Once established, rhombohedral faces grow slowly because a monomolecular layer of strongly bound water forces Ca^{2+} and HCO_3^- ions to adsorb on top of the water layer (Stipp, 1999), thus preventing contact between the ions and the solid mineral except at crystal edges. The rhombohedron surfaces thus grow from the edges, so recrystallization of calcite is not controlled by surface area. Thermal energy promotes the process, so that rhombohedra become larger and more equant with burial (Scholle, 1977; Jørgensen, 1986).

Another thermal energy controlled process is the formation of stylolite-precursors. In oceanic settings where pore water has been sampled down through the sediment column, it can be observed how dispersed smectite with depth apparently dissolves and is replaced by distinct illitic bands, a transformation that involves uptake of magnesium ions, which diffuse from the seawater to the depth of transformation as part of a large scale ion exchange (Fabricius & Borre, 2007). In North Sea chalk, kaolinite probably originates from dissolved detrital feldspar; it can be dispersed in pores, but it may also have precipitated as stylolite precursors (Lind *et al.*, 1994). The associated transport of aluminum in the pore water may be facilitated by complexation with organic acids (Maliva *et al.*, 1999).

Hobert & Wetzel (1989) noticed how the thermal energy-promoted silica diagenesis in deep-sea sediments is associated with induration of calcareous sediments. The transformation from opal-A via opal-CT to micro-quartz involves a stepwise depth-wise

decrease in dissolved silica in the pore water because the stability of the silica phases increases. This process influences solubility and transport of Ca^{2+} ions because these form hydrous complexes with silica (Tanaka & Takahashi 2000).

Both clay diagenesis and silica diagenesis cause changes to the chalk texture. The textural change happens because where the first crystals of the stable phase precipitates, a relatively low concentration of the relevant ions will be present in the pore water and give rise to diffusion from the sites of the less stable phase to the site of the stable phase. In this way silica concretions and stylolite precursors cause the sediment to become less mineralogically mixed. Un-mixing of the silica dispersed in the sediment probably takes place in association with the transformation from opal-A to opal-CT (Fig. 3), while formation of quartz crystals would be initiated by solid state transformation of opal-CT (Hjuler & Fabricius, 2009). The resulting aggregate of tiny quartz crystals can form chert, be dispersed in the pore water as micro-quartz particles or act as cementing phase in chalk (Fig. 4).

Porosity-reducing processes controlled by stress include mechanical (plastic) compaction of carbonate ooze and chalk (e.g. Scholle 1977). It is debated whether pressure dissolution at calcite-calcite contacts, which causes transformation of ooze to chalk, and pressure dissolution at stylolites is controlled by stress or by temperature. From experimental studies of carbonate sediments, Baker *et al.* (1980) found that relief of strain energy caused by stress is a significant factor in dissolution, but also temperature may play a role due to its control on diffusion as discussed by Ehrenberg *et al.* (2016). For chalk, temperature is apparently not a limiting factor for pressure solution at stylolites; Ontong Java Plateau stylolites were found in very cold sediments with temperatures below 15°C (Kroenke *et al.*, 1991; Lind, 1993a). The reason is probably the very small distance needed for diffusion along crystal contacts in the fine-grained chalk, and a system open to diffusion of calcium ions. The latter is indicated in oceanic settings by a gradient in Ca-concentration in the pore water from the depth where stylolites develop to the sea floor as part of the large scale ion exchange (Fabricius & Borre, 2007).

Stress is defined as force per area, but for a porous rock it is not generally accepted which area should be chosen. A simple proxy for stress is burial depth, but that can be misleading especially in situations with overpressure in pores. In several studies this problem is partially solved by subtracting pore pressure or, for indurated sediments, a fraction of pore pressure from total stress due to load of overburden, achieving an approximate 'effective stress' (e.g. Andersen, 1995). As explained below, the 'effect' is actually the elastic deformation, and the effective stress is defined as the product of elastic deformation and the stiffness of the rock. This means that a stiff (highly cemented) rock obtains a higher effective stress but less elastic deformation for a given load as compared to a soft sediment; but stress-driven diagenetic processes progress through elastic deformation of the sediment grains (e.g. Schlanger & Douglas, 1974). In the following sections, a large dataset on pelagic carbonates is presented, to explain how elastic strain can be calculated and demonstrate how elastic strain can give information on the stress-driven diagenetic processes. These include pressure dissolution processes as well as plastic strain causing marked decrease in porosity.

DATA

For the present study, core data from the Ocean Drilling Program (ODP) and core data from selected North Sea fields and water zone intervals are included (Fig. 5; Kroenke *et al*., 1991; Sigurdsson *et al*., 1997; Coffin *et al*., 2000; Fabricius, 2007; Fabricius, 2014). All samples represent pelagic or hemipelagic carbonate sediments and sedimentary rocks with carbonate content above 80%.

The Ocean Drilling Program cores were collected from ODP Site 807 on the Ontong Java Plateau (Kroenke *et al*., 1991), ODP sites 999 and 1001 in the Caribbean Sea (Sigurdsson *et al*., 1997), and ODP Site 1138 on the Kerguelen Plateau (Coffin *et al*., 2000). The samples were classified in accordance with Ocean Drilling Program nomenclature (Mazzulo *et al.,* 1988). According to this nomenclature, carbonate ooze is a pelagic or hemipelagic calcareous sediment that can easily be deformed with fingers. Chalk is a pelagic or hemipelagic calcareous sedimentary rock with a low degree of consolidation, so that it can easily be shaped by a knife. Limestone is a calcareous sedimentary rock with a high degree of

consolidation, so that it can only be scratched by a knife. The samples from Ontong Java Plateau (Figs 2 and 3) include 177 calcareous ooze samples of Miocene to Pleistocene age, 221 chalk samples of Eocene to Miocene age and 54 limestone samples of Upper Cretaceous to Eocene age. The samples from the Caribbean Sea include 3 chalk samples of Eocene age, as well as 55 limestone samples of Upper Cretaceous to Miocene age. The samples from Kerguelen Plateau include nine calcareous ooze samples of Miocene age, 87 chalk samples of Upper Cretaceous to Miocene age and 25 limestone samples of Upper Cretaceous age.

The samples from the North Sea Chalk Group (Figs 1 and 4) include samples from the Dan field, the Gorm field, the Syd Arne field and the Tyra field, as well as water zone samples from various dry exploration wells. All samples from the North Sea Chalk Group are of Upper Cretaceous or Palaeocene (Danian) age, all are sedimentologically described as chalk, but only 16 samples would have been described as chalk according to ODP nomenclature, the remaining 113 samples would be described as limestone (Fabricius, 2007). The North Sea samples include 92 hydrocarbon bearing samples and 12 samples from a water zone. All samples from the North Sea were cleaned for hydrocarbons by Soxhlet extraction before core measurements.

For each sample the following data are used in the present analysis: depth below sea level, h; water depth, h_w; porosity, ϕ; bulk density of water saturated sample, ρ_b; elastic ultrasonic P-wave velocity of water saturated samples, V_P; pore water pressure, P; together with data for bulk modulus, K_c; and shear modulus, G_c, of calcite (see citations in Mavko *et al*. 2009), as well as density, ρ_w and bulk modulus, K_w of pore water estimated from salinity, temperature and pressure according to Batzle & Wang (1992) as cited in Mavko *et al*. (2009).

THEORY AND METHODOLOGY

Burial controlled porosity reduction depends on the weight of the overburden, the degree of cementation and the extent to which the pore fluid pressure counteracts the stress from the overburden. During burial, sediment particles carry a load and will constantly be under

elastic deformation, although loose sediments may additionally react to the load by particles rearranging to a closer packing. By added load, this plastic strain can in principle continue until closest packing is obtained, but in many cases it can be observed that it is halted by contact cementation. In order for physical compaction to resume, a significant extra load needs to be added (Lind, 1993b). This renewed physical compaction is called pore collapse and involves breaking of contact cement and in some cases even fossils, followed by rearrangement of sediment particles. If pore collapse is caused by a stress equal in all directions (hydrostatic stress), it can be pervasive. If the stress field is anisotropic, pore collapse can occur in compaction bands (Issen & Rudnicki, 2001; Wennberg *et al*., 2013). A predominantly vertical stress thus gives rise to horizontal compaction bands (Fig. 3A), while tectonic stress can give rise to inclined compaction bands. Compaction bands can localize and thus predate stylolites (Fig. 6).

Further porosity reduction is caused by stylolite-sourced pore-filling cementation. The load on sediments thus constantly causes elastic and sometimes also plastic deformation.

The overburden load in the vertical direction is counteracted by the pressure in the pore fluid. If the pore fluid cannot drain out during an added load, pore pressure increases. The sediment then acts stiffly, and relatively small elastic deformation takes place. If the pore fluid can drain out of the sediment, the pore pressure still counteracts the load, but the fluid is only compressed by its own load and the pore pressure remains practically constant. [As is common practice in geotechnical engineering, Biot (1941) refers to the drained situation by the strictly speaking incorrect but practical formulation: "water is incompressible".] In the drained case, the sediment becomes softer and more elastic deformation takes place. Whether an undrained or a drained situation arises depends on sediment permeability and rate of deformation. For rapid deformation (as for example due to sonic or ultrasonic elastic waves) most sediments will react undrained, whereas for deformation during burial, only low-permeability layers may be undrained and act as seals, while most sediments above and below the seal act drained. If burial is so rapid that the seal

acts undrained, sediments below the seal can act drained, but with a pore pressure above the hydrostatic pressure. This situation is referred to as regional overpressure.

In the typical drained case, the counteracting effect of the fluid pressure is reduced by a factor α, called Biot's coefficient. The magnitude of α depends on the contact area between particles. In loose sediments, the contact area is relatively small and α will approach (but never reach) unity. Contact cementation reduces α, and pore-filling cementation reduces α even more. For homogeneous sediments, the theoretical minimum value for α is equal to porosity. Biot (1941) defined α in terms of elastic moduli equivalent to (Biot & Willis, 1957):

$$\alpha = 1 - K/K_{\text{min}} \quad (1)$$

where K is the elastic bulk modulus of the sediment under fully drained conditions and K_{min} is the elastic bulk modulus of the mineral constituting the sediment. The bulk modulus describes the elastic deformation of isotropic material resulting from stress that is equal in all directions.

When strain only takes place in the vertical direction (uniaxial strain), the total vertical load on a sediment causes a stress, σ_1, defined as load per horizontal area. In the drained case, the volumetric elastic strain, ε, resulting from a given total vertical stress, σ_1, and a given fluid pressure P, in analogy with Biot (1941) can be described by the elastic modulus, M (Alam *et al*., 2012), where M is the modulus of uniaxial strain, which describes the case where deformation only takes place in the direction of applied load:

$$\varepsilon = (\sigma_1 - \alpha P)/M \quad (2)$$

εM can be referred to as 'effective vertical stress', σ_1', and it sometimes replaces depth in porosity depth plots (e.g. Andersen, 1995):

$$\sigma_1' = \sigma_1 - \alpha P \quad (3)$$

In loose sediments, where α is close to unity, it is in geotechnical engineering common practice to formulate 'effective stress', $\sigma_1{}^t$ in analogy with Terzaghi (1923):

$$\sigma_1{}^t = \sigma_1 - P \quad (4)$$

or:

$$\varepsilon_t = (\sigma_1 - P)/M \quad (5)$$

For chalk, Eq. 2 thus describes the elastic deformation before pore collapse, and Eq. 5 approximates the (higher) elastic deformation after pore collapse (Fig. 7). Pore collapse increases elastic strain because M decreases.

The pore fluid not only affects the resulting deformation due to its pressure, also its chemical composition matters. It has been observed that dry chalk and oil-saturated chalk are stiffer than should be theoretically expected from the stiffness of water-saturated chalk, and for water-saturated chalk the salinity and nature of dissolved ions matter. Several explanations have been attempted, including capillary pressure or chemical dissolution (e.g. Schroeder *et al.*, 1998; Risnes *et al.*, 2005; Katika *et al.*, 2015). Recently Nermoen *et al.* (2018) proposed a simple electrostatic addition to Biot's equation, here as formulated for equal stress in all directions:

$$\sigma' = \sigma_{es} + \sigma_{VdW} = K\varepsilon \quad (6)$$

where σ_{es} is negative and represents the electrostatic repulsion between particles with equal surface charge, and σ_{VdW} represents the stress due to load at smooth crystal contacts (as where particles meet in contact cement).

For the evaluation of *in situ* stress and strain on the data set, the following procedure has been applied; first the modulus of undrained uniaxial strain, M_s, for each water saturated sample is calculated from:

$$M_s = \rho_b V_P^2 \quad (7)$$

Then the iso-frame value, which describes the degree to which the solid supports the frame of the rock, *IF*, is calculated by using a solver function from:

$$K^{HS+} = \left(\frac{\phi + (1-IF)(1-\phi)}{K_{sus} + \frac{4}{3}G_c} + \frac{IF(1-\phi)}{K_c + \frac{4}{3}G_c} \right)^{-1} - \frac{4}{3}G_c \quad (8)$$

$$G^{HS+} = \left(\frac{\phi + (1-IF)(1-\phi)}{\xi} + \frac{IF(1-\phi)}{G_c + \xi} \right)^{-1} - \xi \quad (9)$$

$$\xi = \frac{G_c}{6}\left(\frac{9K_c + 8G_c}{K_c + 2G_c} \right) \quad (10)$$

$$K_{sus} = \frac{\left(\phi + (1-\phi)(1-IF)\right)}{\left(\frac{\phi}{K_w} + \frac{(1-\phi)(1-IF)}{K_c} \right)} \quad (11)$$

$$M_s = K^{HS+} + \frac{4}{3}G^{HS+} \quad (12)$$

This formulation is based on Hashin & Shtrikman (1963) and Fabricius (2007).

Then *K* is estimated from:

$$K = \left(\frac{\phi + (1-IF)(1-\phi)}{\frac{4}{3}G_c} + \frac{IF(1-\phi)}{K_c + \frac{4}{3}G_c} \right)^{-1} - \frac{4}{3}G_c \quad (13)$$

and Biot´s coefficient, α can be calculated:

$$\alpha = 1 - K/K_c \quad (14)$$

In order to obtain total vertical stress, σ_1, bulk density data are summed:

$$\sigma_1 = g\,(\rho_w h_w + ((h_1-h_0)/2+h_0-h_w)\rho_{b0} + \Sigma((h_{n+1} - h_{n-1})/2)\,\rho_{bn}) \qquad (15)$$

Where g is acceleration of gravity, and suffixes (0 to n) refer to samples from shallowest to deepest. For the included ODP sites, bulk density data (0 to n) are available from sea bottom and down, for North Sea, bulk density data (1 to n) are available for samples from the Upper Cretaceous and Lower Palaeogene Chalk Group. The overlying sediments defines a large h_0, with an average bulk density ρ_{b0} = 1980 kg/m^3 (Japsen 1998). Uniaxial elastic strain of an intact rock, ε, can then be calculated from Eq. 2, and elastic strain after pore collapse, ε_t, from Eq. 5.

RESULTS

The compiled data set covers a depth range from the sea floor to nearly 4 km below the sea floor (Fig. 8A and B). Porosity and P-wave velocity respectively show negative and positive overall depth trends, but also exhibit significant scatter. For a depth of 1 km, porosity can be anything between 15% and 45% and P-wave velocity can be anything between 1800 m/s and 4500 m/s (Fig. 8). For the ODP data, distinct depth trends are seen for the four sites. On the Ontong Java Plateau (Site 807) porosity decreases with depth at a relatively low rate and velocity increases at a low rate. The rates are higher for Site 999 in the Caribbean Sea and Site 1138 at the Kerguelen Plateau, and still higher for Site 1001 in the Caribbean Sea. For the North Sea data, relatively clear depth trends of decreasing porosity and increasing velocity are seen for water zone samples. By contrast no trend is observed for hydrocarbon zone data. Porosity for these data is at or above the water zone trend and velocity at or below the water zone trend.

With respect to the relationship between P-wave velocity and porosity, it should be noted that they are negatively correlated, following an overall curved trend from water to calcite, but that a given P-wave velocity corresponds to a 10 to 15 p.u. range of porosity, and a given porosity corresponds to a 500 m/s range in velocity for high porosity increasing to a 1500 m/s range for low porosity (Fig. 8C). For porosity below 30%, data representing the North Sea and data representing ODP Site 1001 in the Caribbean follow a

trend of relatively high velocity for a given porosity as compared to data from the other ODP sites (Fig. 8C). These observations indicate that P-wave velocity contains more information than just mineralogy, pore fluid and porosity. The extra information can be described as degree of induration.

The degree of induration is first quantified by iso-frame modelling, where an *IF* of 1.0 corresponds to the highest possible contribution of solids to carrying the load on a homogeneous rock, and *IF* of 0 corresponds to a suspension where no load is carried (Fig. 9). Samples falling along an iso-frame curve is expected to have same degree of induration but a difference in porosity due to different degree of sorting. Contact cementation will tend to preserve porosity but increase induration (higher *IF*), while pore filling cementation will tend to increase induration and also decrease porosity. Of the studied data, only ODP samples are found to have porosity above 60%, and the range of iso-frame value for these high porosities is narrow: $IF \leq 0.1$. The porosity interval 60 to 45% also only represents ODP samples, some of which have low induration and $IF < 0.1$, but most fall in the range of $0.1 < IF < 0.2$. The porosity interval below 45% represents North Sea samples as well as ODP samples. *IF* varies more but only few samples have $IF < 0.2$ and only few samples have $IF > 0.7$.

In order to quantify effective stress and elastic strain, iso-frame values are now used to model Biot's coefficient (Eqs 13 and 14; Fig. 10). Biot's coefficient is a measure of elastic stiffness for a given mineralogy, and is thus related to the degree of induration. For the studied samples, Biot's coefficient tends to decrease with decreasing porosity (Fig. 10A). Carbonate ooze samples fall in a group with a porosity of 50 to 70% and Biot´s coefficient of $\alpha > 0.995$, while chalk samples have a porosity of 35 to 60% and a Biot's coefficient $0.95 < \alpha < 0.995$, although most chalks also fall in a group with $0.98 < \alpha < 0.995$. The carbonate ooze and chalk groups thus overlap with respect to porosity, but demonstrate a distinct gap with respect to Biot's coefficient (Fig. 10B).

The ODP limestones have porosity below 40% and show a wide range of Biot's coefficient (0.5 to 0.95), but most studied limestones have a value of $\alpha > 0.75$ (Fig. 10A). A clear gap in Biot's coefficient between chalk and limestone is not found, but there are only few data points near $\alpha = 0.95$, and only few data with porosity between 38% and 42%. The North Sea samples, irrespective of representing a hydrocarbon bearing interval or a water zone, tend to have relatively low Biot's coefficient for a given porosity.

The result from modelling elastic strain can be compared to the plastic strain represented by decreasing porosity. When both values are plotted versus effective stress, a relatively smooth trend is found for porosity, while the elastic strain – effective stress plot separates ooze, chalk and limestone in distinct groups (Fig. 11A and B). Only in the ooze interval is a systematic depth-wise increase observed (Fig. 11B). The effective stress is calculated based on Eq. 3 and represents homogeneous sediment or sedimentary rock. The corresponding elastic strain is calculated from Eq. 2 and represents the actual *in situ* elastic strain. Porosity is overall related to effective stress, but for the ODP data, separate trends can be defined for ooze, chalk and limestone, and North Sea samples from the hydrocarbon zone fall on a distinct, high effective stress trend (Fig. 11A). Although the range of porosity is not equally represented by data from the four deep sea sites, representing three oceans, it is worth considering that distinct porosity – effective stress trends cannot be defined based on locality (Fig. 11C). Likewise the grouping according to lithology on the elastic strain plot (Fig. 11B) is not reflected in locality (Fig. 11D).

DISCUSSION

The comparison of plots of porosity and elastic strain versus effective stress for carbonate ooze, chalk and limestone from different localities now allows for the interpretation of porosity-reducing processes in calcareous sediments and rocks (Table 1). At the sea floor, carbonate ooze has porosity of around 70% and Biot's coefficient approaches 1.0. The ooze suffers no elastic strain, only the single particles are hydrostatically compressed by the pressure in the water. As the ooze is buried, effective stress increases due to the weight of

the overlying sediments and elastic strain accordingly increases, while mechanical compaction reduces porosity (Fig. 11A and B). During the mechanical compaction of carbonate ooze, Biot's coefficient remains high (Fig. 10B) while porosity is reduced to around 60% (Figs 10B and 11A). The porosity reduction happens over a long depth interval of 200 to 300 m (e.g. Schlanger & Douglas 1974). One reason for the thick ooze interval is that the particles repel one another due to ions adsorbed on equivalent mineralogical faces as documented by Meireles *et al*. (2020). These authors found that calcite powder settled in saltwater has *ca* 10% higher porosity than calcite powder settled in inert fluid. This repulsion contrasts with the perception of interparticle electrostatic attraction (cohesion) (Gabrowski *et al*., 2011; Schieber *et al*. 2013; Bulls *et al*., 2017).

In order to overcome electrical repulsion, a high load at particle contacts is required, so when the ooze indurates into chalk, the ooze particles are consequently subjected to an elastic strain of up to 0.003 (i.e. 0.3%) (Fig. 11B). This strain corresponds to a stress at grain contacts in the order of 0.3 GPa; a stress level where Croize *et al*. (2010) found pressure solution between calcite crystals. So the early pore-stiffening cementation is probably typically the consequence of pressure solution. The observed drop in Biot's coefficient indicates that this contact cementation increases the grain-contact area (Fig. 10B). Consequently the elastic strain drops drastically and the porosity remains close to 50% in the following depth interval (Fig, 11A and B). High heat-flow may facilitate contact cementation at lower stress, as was found for ODP Site 504 near the Costa Rica Rift, where the carbonate was found to have stiffened with high porosity (Wetzel, 1989). The reason is probably enhanced recrystallization, consequent larger crystals and less effect of charge on crystal surfaces. This would mean that the stiffening in this case took place as a consequence of recrystallization alone (Borre & Fabricius, 1998).

In the chalk interval, added load can lead to breakage of contact cement and cause pore collapse (e.g. Lind, 1993b). Pore collapse can cause localized compaction bands (Fig. 6) or pervasive brecciation as seen in highly porous intervals in North Sea chalk (Hardman, 1982). The effective stress interval corresponding to the chalk interval varies

among different locations. For the data from the Caribbean Sea (Sites 999 and 1001) and the Kerguelen Plateau (Site 1138), the transition from chalk to limestone takes place at a relatively low effective stress. For the Ontong Java Plateau (Site 807) and possibly the North Sea at a higher effective stress (Fig. 11B and D). This indicates that the transition from chalk to limestone is controlled by temperature rather than stress, probably because of the association with silica diagenesis described in the *Introduction* to this paper. Because only little cementation takes place in the chalk interval and porosity reduction probably is controlled by mechanical compaction in compaction bands, elastic strain builds up with increasing effective stress, in the Ontong Java Plateau to as much as 0.003 (i.e. 0.3%; Fig. 11B and D). This strain is calculated from Eq. 2 and applies to the clean chalk. It again corresponds to the stress required for calcite-calcite pressure solution (Croize *et al*., 2010) and it also indicates that at the transition from chalk to limestone some calcite-calcite pressure dissolution can take place, but typically the source of cementing ions would be dissolution at stylolites.

If no cement holds the sedimentary rock together, as would be the case following pore collapse or at stylolite precursors/stylolites; Biot's coefficient approaches 1.0, and the effective stress decreases (Eq. 4), but the elastic strain increases because elastic modulus, M, decreases at a higher rate (Eq. 5). Based on a chosen very low (IF = 0.01) iso-frame value, the post-pore collapse elastic modulus and elastic strain is modelled and plotted on Fig. 11B as tiny dots. In order to allow comparison with corresponding intact rock, the effective stress is plotted as calculated from Eq. 3. The modelled strain data trend fall in a continuation of the ooze trend, and the involved elastic strains are very high – above 0.01 (maximal ε_t = 0.03) at the transition from chalk to limestone (Fig. 11B). This indicates that while the clay diagenesis creating stylolite precursors probably is temperature controlled, pressure dissolution of calcite at contact with clay minerals of the stylolite-precursor and consequent stylolite development is probably stress controlled. In the limestone interval, the progressing pore-filling cementation causes higher strength of the sedimentary rock, increasing grain contact area, and consequently elastic strain decreases with increasing effective stress, while the high strain at the stylolites prevails (Fig. 11B). The low elastic

strain explains why pore collapse and compaction bands have not been documented in these limestones.

Temperature and stress thus have distinct roles in burial diagenesis. Thermal energy changes the minerals and can facilitate or impede the stress-driven porosity loss. The transition from ooze to chalk is typically stress driven via calcite–calcite pressure dissolution and follows after a depth-interval of mechanical compaction; but where heat flow is high, recrystallization can cause early stiffening and preservation of high porosity. The transition from chalk to limestone is facilitated by stylolite-precursors, where calcite will be highly strained and dissolve, but the stylolite precursors need thermal energy to be formed. In the absence of these, the transition is delayed until strain is high enough for renewed calcite–calcite pressure dissolution. Insufficient thermal energy can delay the consequent pore filling cementation in the presence of opal, because Ca-ions released by pressure dissolution at stylolites and calcite–calcite contacts can be held in solution by silica-complexes until the thermal-energy controlled transformation of opal to quartz, which is associated with a drop in concentration of dissolved silica.

The outlined modelling of *in situ* elastic strain in intact sedimentary rock as well as following pore collapse highlights the amount of elastic strain suffered by unconsolidated sediments while they undergo mechanical compaction, and it quantifies the strain relaxation associated with contact cementation and pore filling cementation. The method has the potential to predict pore collapse from geophysical data following changes in effective stress due to added load or decrease in pore pressure. This is relevant for exploration and production of hydrocarbons from chalk targets, where decrease in pore pressure typically occurs.

CONCLUSIONS

Stress-related diagenetic processes in sedimentary rocks can be described in terms of elastic strain. The reason is that these diagenetic processes are controlled by the stress on the grain

contacts, while effective stress is conventionally normalized to the entire cross-sectional area. The strain is independent of choice of reference area.

The studied core data from calcareous ooze, chalk and limestone (indurated chalk) from three oceans and from the North Sea basin, indicate that an elastic strain of 0.3% is critical for the onset of calcite–calcite pressure dissolution in ooze at transition to chalk, and probably also in chalk at the transition to limestone. In the chalk section, the onset of stylolite development happens at an elastic strain of the calcite crystals of *ca* 2% in contact with clay minerals. This causes continuous pressure dissolution and a source of calcite for pore-filling cementation.

During burial, elastic strain builds up in ooze until the critical 0.3%, and then contact cementation leads to stress release and the transition to chalk. In the chalk section, elastic strain builds up again during burial before the abrupt transition to limestone. By contrast to the situation in soft sediments, burial and increasing pore-filling cementation in the limestone leads to a decline in elastic strain with depth.

ACKNOWLEDGEMENTS

This research used data provided by the Ocean Drilling Program (ODP). The ODP is sponsored by the US National Science Foundation (NSF) and participating countries under management of Joint Oceanographic Institutions (JOI), Inc. Morten Leth Hjuler and three anonymous reviewers are thanked for critically reading the manuscript.

DATA AVAILABILITY STATEMENT

The data that support the findings of this study are openly available in the publications cited in the DATA section of the paper.

REFERENCES

Alam, M.M., **Fabricius, I.L.** and **Christensen, H.F.** (2012) Static and dynamic effective stress coefficient of chalk. *Geophysics*, **77**, L1–L11.

Andersen, M.A. (1995) *Petroleum Research in North Sea Chalk*. RF-Rogaland Research. Joint Chalk Research Program Phase IV, Stavanger, 179 pp.

Anderskouv, K. and **Surlyk, F.** (2012) The influence of depositional processes on the porosity of chalk. *J. Geol. Soc.*, **169**, 311–325.

Andreassen, K.A. and **Fabricius, I.L.** (2010) Biot critical frequency applied to description of failure and yield of highly porous chalk with different pore fluids. *Geophysics*, **75**, E205–E213.

Baker, P.A., Kastner, M., Byerelee, J.D. and **Lockner, D.A.** (1980) Pressure solution and hydrothermal recrystallization of carbonate sediments –an experimental study. *Mar. Geol.*, **38**, 185-203.

Batzle, M. and **Wang, Z.** (1992) Seismic properties of pore fluids. *Geophysics*, **57**, 1396–1408.

Berger, W.H., **Kroenke, L.W.**, **Mayer, L.A.**, **Backman, J.**, **Janecek, T.R.**, **Krissek, L.**, **Leckie, M.** and **Lyle, M.** (1992) The record of Ontong Java Plateau - main results of ODP Leg 130. *Geol. Soc. Am. Bull.*, **104**, 954–972.

Biot, M.A. (1941) General Theory of Three-Dimensional Consolidation. *J. Appl. Phys.*, **12**, 155–164.

Biot, M.A. and **Willis, D.G.** (1957) The elastic coefficients of the theory of consolidation. *J. Appl. Mech.*, **24**, 594–601.

Black, M. (1963) Function and fine-structure in protista: 2. The fine structure of the mineral parts of coccolithophoridae. *Proc. Linnean Soc. London*, **174**, 41–46.

Bolton, C. T., **Hernández-Sánchez, M.T.**, **Fuertes, M.-A.**, **González-Lemos , S.**, **Abrevaya, L.**, **Mendez-Vicente, A.**, **Flores, J.-A.**, **Probert, I.**, **Giosan, L.**, **Johnson, J.** and **Stoll, H.M**. (2016) Decrease in coccolithophore calcification and CO_2 since the middle Miocene. *Nature Comm.* **7,** Article number: 10284 (2016).

Borre, M. and **Fabricius, I.L.**, (1998) Chemical and mechanical processes during burial diagenesis of chalk: An interpretation based on specific surface data of deep-sea sediments. *Sedimentology*, **45**, 755–769.

van Buchem, F.S.P., **Smit, F.W.H.**, **Buijs, G.J.A.**, **Trudgill, B.** and **Larsen, P.-H.** (2017) Tectonostratigraphic framework and depositional history of the Cretaceous–Danian succession of the Danish Central Graben (North Sea) – new light on a mature area. *Geol. Soc. London, Petroleum Geol. Conf. series*, **8**, 9–46.

Buls, T., **Anderskouv, K.**, **Friend, P.L.**, **Thompson, C.R.L.** and **Stemmerik, L.** (2017) Physical behaviour of Cretaceous calcareous nannofossil ooze: Insight from flume studies of disaggregated chalk. *Sedimentology*, **64**, 478–507.

Burns, D.A. (1975) Changes in nannofossil morphology by diagenetic processes in cretaceous chalk deposits. *N Z J. Geol. Geophys.*, **18**, 469–476.

Coffin, M.F., **Frey, F.A.**, **Wallace, P.J.**, *et al.* (2000) *Proc. ODP, Init. Repts.*, **183** [Online]. www-odp.tamu.edu/publications/183_IR/183ir.htm.

Cooke, P.J., **Nelson, C.S.**, **Crundwell, M.P.**, **Field, B.D.**, **Elkington, E.S.** and **Stone, H.H.** (2004) Textural variations in Neogene pelagic carbonate ooze at DSDP Site 593, southern Tasman Sea, and their paleoceanographic implications. *N Z J. Geol. Geophys.*, **47**, 787–807.

Crabtree, B., **Fritsen, A.**, **Mandzuich, K.**, **Moe, A.**, **Rasmussen, F.**, **Siemers, T.**, **Soiland, G.** and **Tirsgaard, H.** (1996) Description and classification of chalks, North Sea region. *Norwegian Petroleum Directorate Spec. Pub.* Stavanger, 145 pp.

Croizé, D., **Renard F.**, **Bjørlykke, K.** and **Dysthe, D.K.** (2010) Experimental calcite dissolution under stress: Evolution of grain contact microstructure during pressure solution creep. *J. Geophys. Res.*, **115** (B9).

D'Heur, M. (1984) Porosity and hydrocarbon distribution in the North Sea chalk reservoirs. *Mar. Pet. Geol.*, **1**, 211–238.

Dunham, R.J. (1962) Classification of carbonate rocks according to depositional textures. *AAPG Spec. Pub.*, **1**, 108–121.

Ehrenberg, S.N., Moradi, S., Yaxin, L. and **Chen R.** (2016) Stylolites and porosity in a Lower Cretaceous limestone reservoir, onshore Abu Dhabi, U.A.E. *J. Sediment. Res.* **86**, 1228-1247.

Ehrmann, W.U. (1986) Die Maastricht-Stufe in NW-Deutschland. Teil 7. Zum Sedimenteintrag in das zentrale nordwesteuropäische Oberkreidemeer. *Geologisches Jahrbuch, A*, **97**, 3–139.

Fabricius I.L. (2007) Chalk: composition, diagenesis and physical properties. *Bull. Geol. Soc. Denmark*. **55**, 97–128.

Fabricius, I.L. (2014) Burial stress and elastic strain of carbonate rocks. *Geophys. Prosp.*, **62**, 1327–1336.

Fabricius, I.L. and **Borre, M.K.** (2007) Stylolites, porosity, depositional texture, and silicates in chalk facies sediments. Ontong Java Plateau–Gorm and Tyra fields, North Sea. *Sedimentology*, **54**, 183–205.

Fabricius, I.L., **Høier, C.**, **Japsen, P.** and **Korsbech, U.** (2007a) Modelling elastic properties of impure chalk from South Arne Field, North Sea. *Geophys. Prosp.*, **55**, 487–506.

Fabricius, I.L., **Røgen, B.** and **Gommesen, L.** (2007b) How depositional texture and diagenesis control petrophysical and elastic properties of samples from five North Sea chalk fields. *Petroleum Geoscience*, **13**, 81–95.

Faÿ-Gomord, O., **Soete, J.**, **Katika, K.**, **Galaup, S.**, **Caline, B.**, **Descamps, F.**, **Lasseur, E.**, **Fabricius, I.L.**, **Saïag, J.**, **Swennen, R.** and **Vandycke, S.** (2016) New insight into the microtexture of chalks from NMR analysis. *Mar. Pet. Geol.*, **75**, 252–271

Gale, A.S. (2000) The Cretaceous World. In: *Biotic Response to Global Change. The Last 145 Million Years* (Eds S.J. Culver and P.F. Rawson), Cambridge University Press, Cambridge, 4–19.

Grabowski, R.C., **Droppo, I.G.** and **Wharton, G.** (2011) Erodibility of cohesive sediment: the importance of sediment properties. *Earth-Sci. Rev.*, **105**, 101–120.

Håkansson, E., **Bromley, R.** and **Perch-Nielsen, K.** (1974) Maastrichtian Chalk of North-West Europe—a Pelagic Shelf Sediment. In: *Pelagic Sediments: on Land and under the Sea* (Eds K.J. Hsu and H.C. Jenkyns) *IAS Spec Pub*, **1**, 211–233.

Hansen, T. and Surlyk, F. (2014) Marine macrofossil communities in the uppermost Maastrichtian chalk of Stevns Klint, Denmark. Palaeo Palaeo Palaeo, 399, 323–344.

Hardman, R.F.P. (1982) Chalk reservoirs of the North Sea. *Bull. geol. Soc. Denmark*, **30**, 119-137.

Hashin, Z. and **Shtrikman, S.** (1963) A variational approach to the elastic behavior of multiphase materials: *J. Mech. Phys. Solids*, **11**, 127–140.

Hasiuk, F.J., **Kaczmarek, S.E.** and **Fullmer, S.M.** (2016) Diagenetic origins of the calcite microcrystals that host microporosity in limestone reservoirs. *J. Sed. Res.*, **86**, 1163–1178.

Hatton, I.R. (1986) Geometry of allochthonous Chalk Group members, Central Trough, North Sea. *Mar. Pet. Geol.*, **3**, 79–98.

Hjuler, M.L. and **Fabricius, I.L.** (2009) Engineering properties of chalk related to diagenetic variations of Upper Cretaceous onshore and offshore chalk in the North Sea area. *J. Petroleum Sci. Eng.*, **68**, 151–170.

Hobert, L.A. and **Wetzel, A.** (1989) On the relationship between silica and carbonate diagenesis in deep-sea sediments. *Geologische Rundschau* **78**, 765-778.

Issen, K.A. and **Rudnicki, J.W.** (2001) Theory of Compaction Bands in Porous Rock. *Phys. Chem. Earth (A)*, **26**, 95–100.

Japsen P. (1998) Regional Velocity-Depth Anomalies, North Sea Chalk: A record of overpressure and Neogene uplift and erosion. *AAPG Bull.*, **82**, 2031–2074.

Jørgensen, N.O. (1986) Geochemistry, diagenesis and nannofacies of chalk in the North Sea Central Graben. *Sed. Geol.*, **48**, 267–294.

Katika, K., **Addassi, M.**, **Alam, M.M.** and **Fabricius, I.L.** (2015) The effect of divalent ions on the elasticity and pore collapse of chalk evaluated from compressional wave velocity and low-field Nuclear Magnetic Resonance (NMR). *Petroleum Sci. Eng.*, **136**, 88–99.

Kennedy, W.J. (1980) Aspects of chalk sedimentation in the southern Norwegian offshore. *The sedimentation of the North Sea reservoir rocks.* Norwegian Petroleum Society. Paper IX, 29 pp.

Korsbech, U., Aage, H., Hedegaard, K., Andersen, B.L. and **Springer, N.** (2006) Measuring and modelling the displacement of connate water in chalk core plugs during water injection. *SPE Reserv. Eval. Eng.*, **9**, 259-265.

Kroenke, L.W., **Berger, W.H.**, **Janecek, T.R.** *et al.* (1991) *Proc. ODP, Init. Repts.*, **130**, College Station, TX (Ocean Drilling Program), 1240 pp.

Lind, I.L. (1993a) Stylolites in chalk from Leg 130, Ontong Java Plateau. In Berger, W.H., Kroenke, L.W., Mayer, L.A. *et al.*, *Proc. ODP, Sci. Results*, **130**: College Station, TX (Ocean Drilling Program), 445–451.

Lind, I.L. (1993b) Loading experiments on carbonate ooze and chalk from Leg 130, Ontong Java Plateau. In Berger, W.H., Kroenke, L.W., Mayer, L.A., *et al*., *Proc. ODP, Sci. Results*, **130**: College Station, TX (Ocean Drilling Program), 673–686.

Lind, I., Nykjær, O., Priisholm, S. and **Springer, N.** (1994) Permeability of stylolite-bearing chalk. *J. Petrol. Technol.*, **46**, 986–993.

Lopatin, N.V. (1971) Temperature and time as factors of coalification. *Izvestiya Akademii Nauk SSSR, Seriya gelogicheskaya* (in Russian), **3**, 95-106.

Madsen, H.B. and **Stemmerik, L.** (2010) Diagenesis of Flint and Porcellanite in the Maastrichtian Chalk at Stevns Klint, Denmark. *J. Sed. Res.*, **80**, 578–588.

Maliva, R.G. and **Dickson, J.** (1992) Microfacies and diagenetic controls of porosity in Cretaceous/Tertiary chalks, Eldfisk field, Norwegian North Sea. *AAPG Bull.*, **76**, 1825–1838.

Maliva, R.G., **Dickson, J.A.D.** and **Fallick, A.E.** (1999) Kaolin cements in limestones: potential indicators of organic-rich pore waters during diagenesis. *J. Sed. Res.*, **69**, 158–163.

Mallon, A.J. and **Swarbrick, R.E.** (2002) A compaction trend for non-reservoir North Sea Chalk. *Mar. Pet. Geol.*, **19**, 527–539.

Mavko, G., **Mukerji, T.** and **Dvorkin, J.** (2009) *The Rock Physics Handbook*. 2nd ed., Cambridge University Press, 511 pp.

Mazzulo, J., **Meyer, A.** and **Kidd, R.** (1988) New sediment classification scheme for the Ocean Drilling Program. In: *Handbook for Shipboard Sedimentologists* (Eds J. Manzullo and A.G. Graham), Texas A&M University, *Ocean Drilling Program, Technical Note*, **8**, 45– 67.

Meireles, L.T.P., **Storebø, E.M.** and **Fabricius, I.L.** (2020) Porosity effects of electrostatic forces in saturated mineral powders. *Geophysics,* **85**, MR37-MR50.

Meyer, A.G., Stemmerik, L., Frykman, P., Buls, T. and **Nourani, M.** (2019) Modifications of chalk microporosity geometry during burial – An application of mathematical morphology. *Mar Petrol. Geol.*, **100**, 212-224.

Nermoen, A., **Korsnes, R.I.**, **Storm, E.V.**, **Stødle, T.I.B.**, **Madland, M.V.** and **Fabricius, I.L.** (2018). Incorporating electrostatic effects into the effective stress relation — Insights from chalk experiments. *Geophysics*, **83**, MR123–MR135.

Neugebauer, J. (1974) Some Aspects of Cementation in Chalk . In: *Pelagic Sediments: on Land and under the Sea* (Eds K.J. Hsu and H.C. Jenkyns) *IAS Spec Pub*, **1**, 149–176.

Patsoules, M. and **Cripps, J.** (1982) The application of resin impregnation to the three-dimensional study of chalk pore geometry. *Eng. Geol.*, **19**, 15–27.

Risnes, R., Madland, M.V., Hole, M. and Kwabiah, N. K. (2005) Water weakening of chalk—Mechanical effects of water-glycol mixtures. *J. Petrol. Sci. Eng.*, **48**, 21–36.

Rouquerol, J., Avnir, D., Fairbridge, C.W., Everett, D.H., Haynes, J.H., Pernicone, N., Ramsay, J.D.F., Sing, K.S.W. and **Unger, K.K.** (1994) Recommendations for the characterization of porous solids. *Pure & Appl. Chem.*, **66**, 1739-1758.

Saïag, J., Collin, P.-Y., Sizun, J.-P., Herbst, F., Faÿ-Gomord, O., Smith, C. C. Caline, B. and **Lasseur, E.** (2019) Classifying chalk microtextures: Sedimentary versus diagenetic origin (Cenomanian–Santonian, Paris Basin, France). *Sedimentology*, **66**, 2976–3007.

Schieber, J., **Southard, J.B.**, **Kissling, P.**, **Rossman, B.** and **Ginsburg, R.** (2013) Experimental deposition of carbonate mud from moving suspensions: importance of flocculation and implications for modern and ancient carbonate mud deposition. *J. Sed. Res.*, **83**, 1025–1031.

Schlanger, S.O. and **Douglas, R.G.** (1974) The pelagic ooze-chalk-limestone transition and its implications for marine stratigraphy. In: *Pelagic Sediments: on Land and under the Sea* (Eds K.J. Hsu and H.C. Jenkyns) *IAS Spec Pub*, **1**, 117-148.

Scholle, P.A. (1977) Chalk diagenesis and its relation to petroleum exploration: oil from chalks, a modern miracle? *AAPG Bull.*, **61**, 982–1009.

Schroeder, C., Bois, A.-P., Maury, V. and **Halle, G.** (1998) Results of tests performed in laboratory on Lixhe chalk to calibrate water/ chalk models. Water/chalk (or collapsible soil) interaction — Part 2. *EurockT98: SPE/ ISRM Programme Committee*, 505–514.

Sigurdsson, H., **Leckie, R.M.**, **Acton, G.D.** *et al.* (1997) *Proc. ODP, Init. Repts.*, **165**, College Station, TX (Ocean Drilling Program), 862 pp.

Stipp, S.L.S. (1999) Toward a conceptual model of the calcite surface: hydration, hydrolysis, and surface potential. Geochim Cosmochim Acta, 63, 3121–3131.

Tanaka, M. and **Takahashi, K.** (2000) The identification and characterization of silicate complexes in calcium chloride solution using fast atom bombardment mass spectrometry. *Anal. Chim. Acta*, **411**, 109–119.

Terzaghi, K. (1923) Die Beziehungen zwischen Elastizitat und Innendruck: *Sitzungsberichte, Akademie der Wissenschaften, K I. IIa*, **132**, 105–121.

Urmos, J., **Wilkens, R.H.**, **Bassinot, F.**, **Lyle, M.**, **Marsters, J.C.**, **Mayer, L.A.** and **Mosher, D.C.** (1993) Laboratory and well-log velocity and density measurements from the Ontong Java Plateau: new insitu corrections to laboratory data for pelagic carbonates. In (Eds W.H. Berger, L.W. Kroenke, L.A. Mayer, T.R. Janecek *et al.*), Proc. ODP, Sci. Results: College Station, TX (Ocean Drilling Program), **130**, 607–622.

Waples, D.W. (1980) Time and temperature in petroleum formation: application of Lopatin's method to Petroleum Exploration. *AAPG Bull.*, **64**, 916-926.

Wennberg, O.P., **Casini, G.**, **Jahanpanah, A.**, **Lapponi, F.**, **Ineson, J.**, **Wall, B.G.** and **Gillespie, P.** (2013) Deformation bands in chalk, examples from the Shetland Group of the Oseberg Field, North Sea, Norway. *J. Struct. Geol.*, **56**, 103–117.

Wetzel, A. (1989) Influence of heat flow on ooze/chalk cementation: Quantification from consolidation parameters in DSDP sites 504 and 505 sediments: *J. Sed. Petrol.*, **59**, 539–547.

Wise Jr., S.W. and **Kelts, K.R.** (1972) Inferred diagenetic history of a weakly silicified deep sea chalk. *GCAGS Transactions*, **22**, 177–203.

FIGURE CAPTIONS

Fig. 1. Backscatter electron micrographs of samples from the water zone of the North Sea Chalk Group [300 μ by 400 μ (left) and magnified central part: 30 μ by 40 μ (right)]. The images illustrate how, when microfossils are cemented, depositional texture influences sorting and hence porosity. (**A**) Chalk mudstone predominantly composed of diagenetically modified nannofossils and nannofossil debris (22% porosity). (**B**) Wackestone predominantly composed of diagenetically modified nanofossils and nannofossil debris as well as partially cemented microfossils (14% porosity). (C) Packstone predominantly composed of partially cemented microfossils as well as diagenetically modified nanofossils and nannofossil debris (9% porosity).

Fig. 2. Backscatter electron micrographs of samples of calcareous sediments and sedimentary rocks from the Ontong Java Plateau [300 μ by 400 μ (left) and magnified central part: 30 μ by 40 μ (right)]. The images illustrate the effect on porosity of burial diagenesis and a stylolite. (**A**) Pleistocene carbonate ooze predominantly composed of calcareous nannofossils and microfossils [10 metres below sea floor (mbsf); 70% porosity]. (**B**) Oligocene chalk predominantly composed of diagenetically modified nannofossils and microfossils, some microfossils appear broken (arrow) (780 mbsf; 54% porosity). (**C**) Upper Cretaceous limestone predominantly composed of heavily diagenetically modified nannofossils and microfossils. A stylolite (s) with a drape of smectite-illite clay transects the rock (1275 mbsf; 20% porosity).

Fig. 3. Backscatter electron micrographs of samples form Ontong Java Plateau [300 μ by 400 μ (left) and magnified central part: 30 μ by 40 μ (right)]. The images illustrate a compaction band and earlier part of silica diagenesis in chalk. (**A**) Miocene chalk with compaction band and opaline fossil fragments, (o) (508 mbsf). (**B**) Eocene chalk with collapse structure (c) associated with degraded opaline fossils (914 mbsf). (**C**) Eocene chalk with degraded opaline fossils (darker grey; o) and neomorphic opal-CT (lighter grey; ct) (1006 mbsf).

Fig. 4. Backscatter electron micrographs of samples from the water zone of the North Sea Chalk Group [300 μ by 400 μ (left) and magnified central part: 30 μ by 40 μ (right)]. The images illustrate the later part of silica diagenesis in chalk. (**A**) Neomorphic micro-quartz,

(q), in chalk pores. (**B**) Neomorphic kaolinite, (k), and micro-quartz replacing possible siliceous fossil fragment. (**C**) Chalk cemented by quartz, (q).

Fig. 5. Locations from where samples were collected (modified after http://www-odp.tamu.edu/sitemap/sitemap.html).

Fig. 6. Stylolite following compaction bands (photo: Ida Lind, Tidsskriftet Varv 1993, 2, front page).

Fig. 7. Mean effective stress – generalized shear stress (*p–q)* diagram displaying area of elastic deformation, limit for failure (formation of fractures: steep solid line) and yield envelope where compaction bands form. Yield under hydrostatic conditions causes pervasive pore collapse. The figure compares the diagram for a strong (1) and a weak (2) sample. The dotted lines show experimental stress paths needed for constructing the diagram. Mean effective stress. $p' = \frac{1}{3}\left(\sigma'_1 + \sigma'_2 + \sigma'_3\right)$. Generalized shear stress, $= \frac{1}{\sqrt{2}} \sqrt{(\sigma_1 - \sigma_2)^2 + (\sigma_2 - \sigma_3)^2 + (\sigma_1 - \sigma_3)^2}$, where $\sigma_1, \sigma_2, \sigma_3$ are the three principal stresses (Andreassen & Fabricius, 2010).

Fig. 8. Cross-plots of raw data for the studied samples annotated with sample location. (**A**) Porosity versus depth below sea floor (mbsf). (**B**) P-wave velocity, V_P, of water saturated samples versus depth (mbsf). (**C**) V_P versus porosity.

Fig. 9. Cross-plot of P-wave modulus of water saturated samples and porosity. The type curves refer to iso-frame value 0 (lowest) to 1.0 (uppermost).

Fig. 10. (**A**) Cross-plot of Biot's coefficient and porosity. (**B**) Detail of uppermost part of (**A**).

Fig. 11. Cross-plots of porosity (**A**) and (**C**) and elastic strain (**B**) and (**D**) versus effective stress; annotated with respect to lithology (**A**) and (**B**) and locality (**C**) and (**D**). (**B**) An interpretation of how effective stress and elastic strain reflect diagenetic processes. Circles represent elastic strain calculated according to Biot (Eq. 2). Tiny dots represent modelled strain at the same samples after a thought pore collapse causing elastic modulus to drop and strain to increase.

Table 1. Generalized burial diagenetic chart for pelagic carbonates.

Properties and processes at lithological interfaces or intervals	**Lithology as a function of burial**	**Porosity**	**Biot's coefficient**	**Temperature controlled diagenetic process**	**Stress controlled diagenetic processes**	
					Porosity-changing process	***In situ* elastic strain**
Interface	Sea floor	70%	→1.0	–	–	0
Interval	Carbonate ooze	–	–	Recrystallization	Mechanical compaction	Elastic strain increases with depth
Interface	Ooze/ chalk transition	60%	0.995	–	Pressure dissolution at calcite – calcite contacts. Contact cementation	Elastic strain drops: 0.01 → 0.001
Interval	Chalk	–	–	Opal-A → Opal-CT Smectite → illite. Clay minerals precipitate in bands	Pore collapse and compaction bands	Elastic strain increases with depth
Interface	Chalk / limestone transition	40%	0.95	Opal-CT → Quartz	Pressure dissolution at calcite – clay mineral contacts. Stylolites form	Elastic strain drops: 0.003 → 0.001

Interval	Limestone	–	–	–	Pore filling cementation	Elastic strain is low

Fig. 12. Generalized burial diagenetic chart for pelagic carbonates.

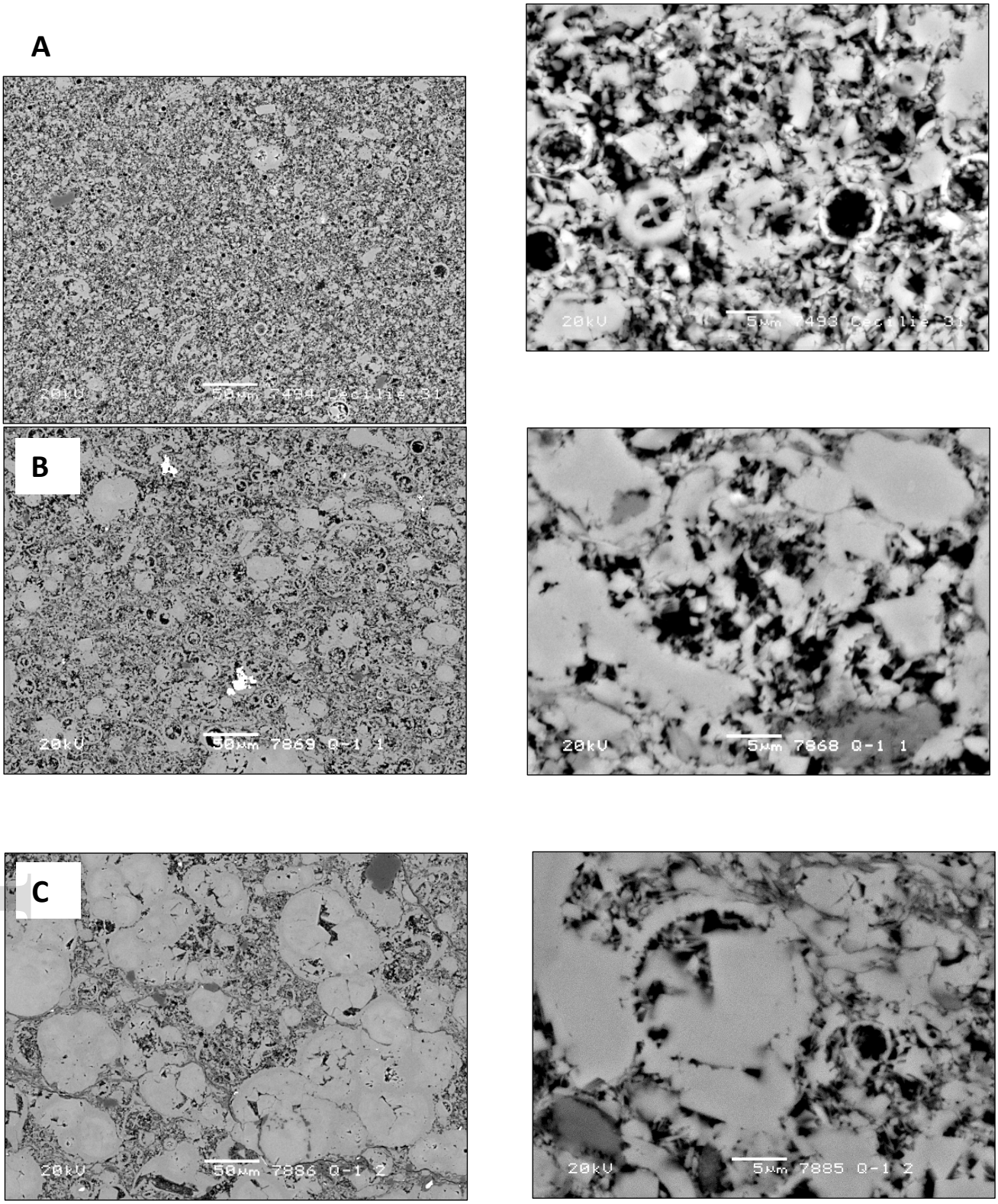

Porosity in chalk - figures

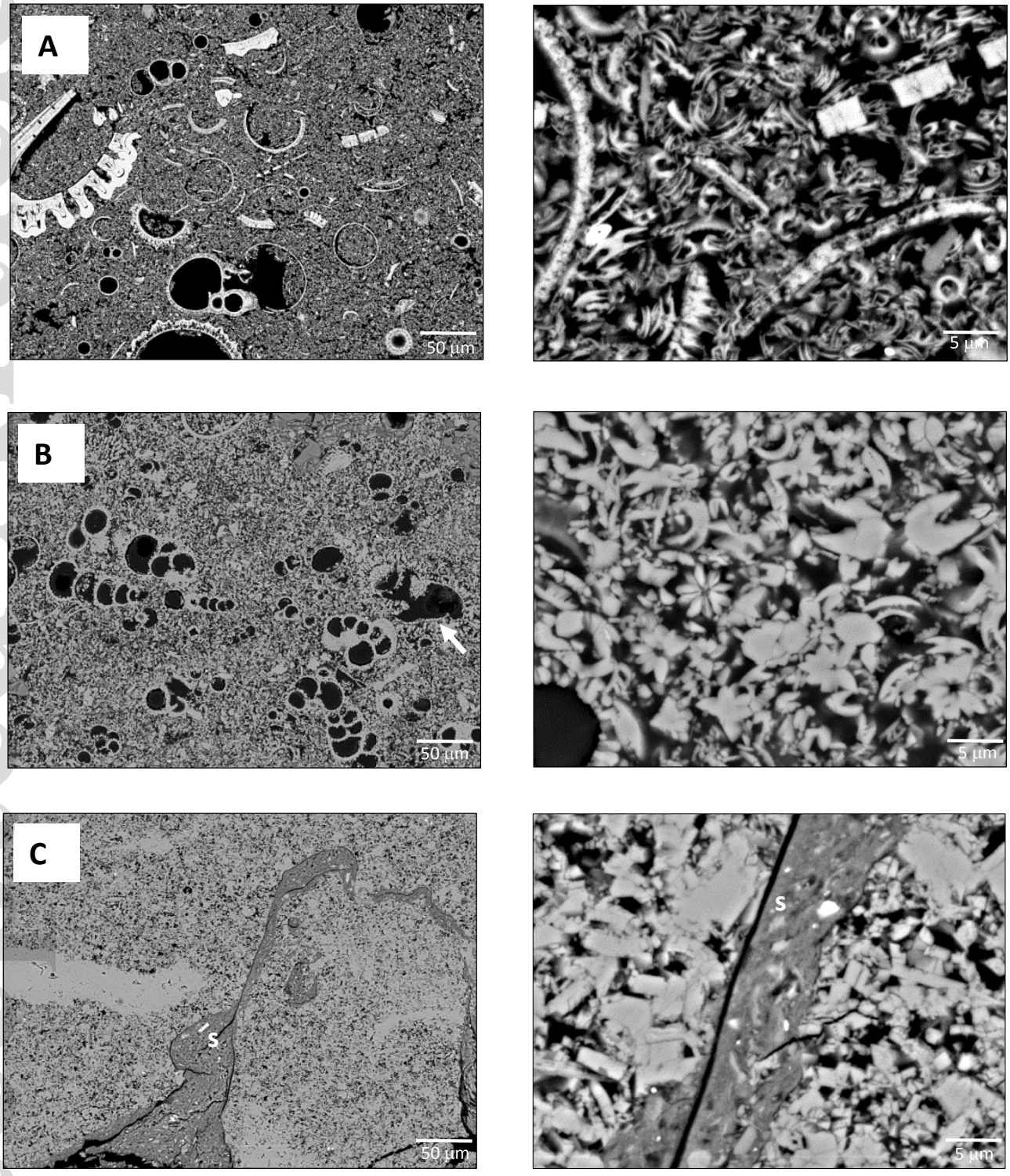

Porosity in chalk - figures

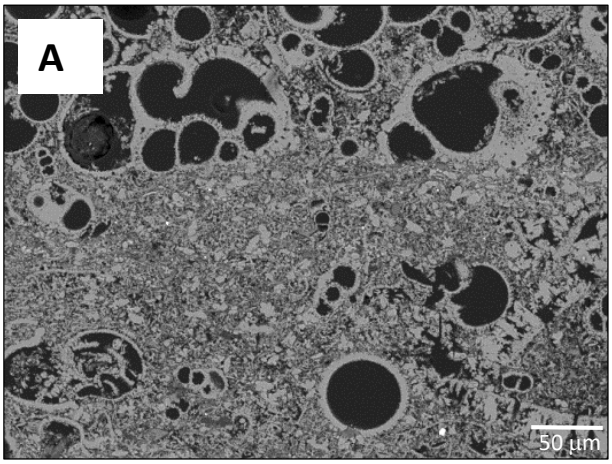

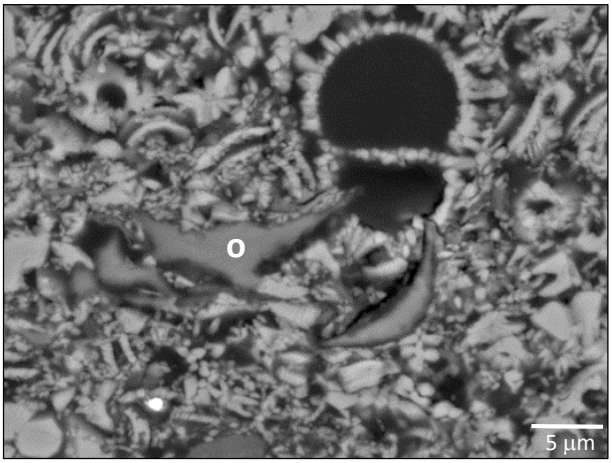

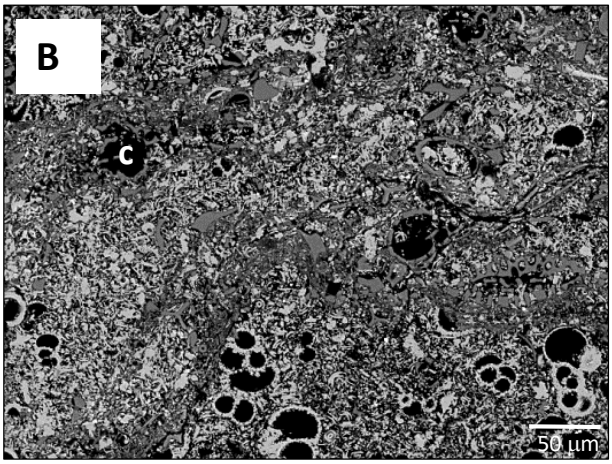

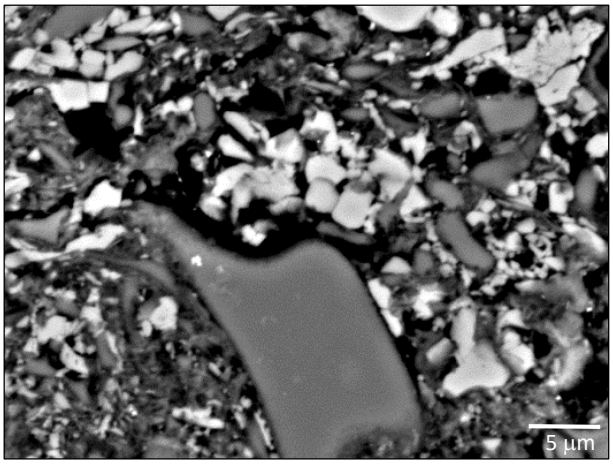

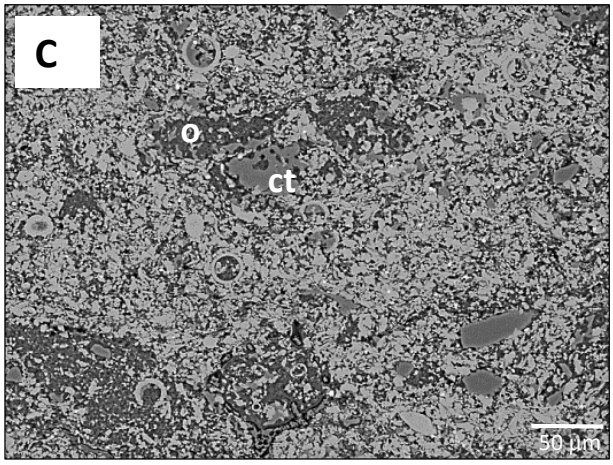

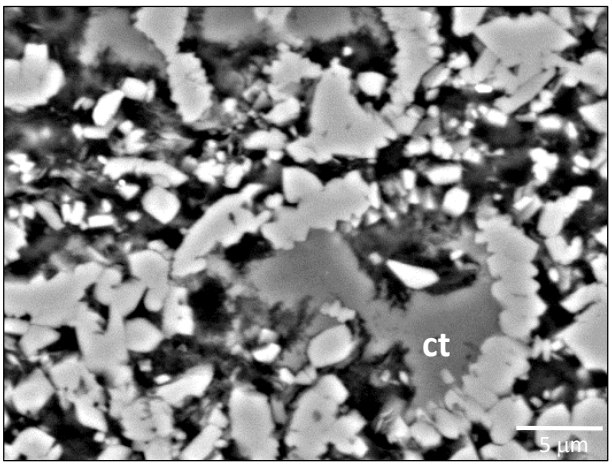

Porosity in chalk - figures

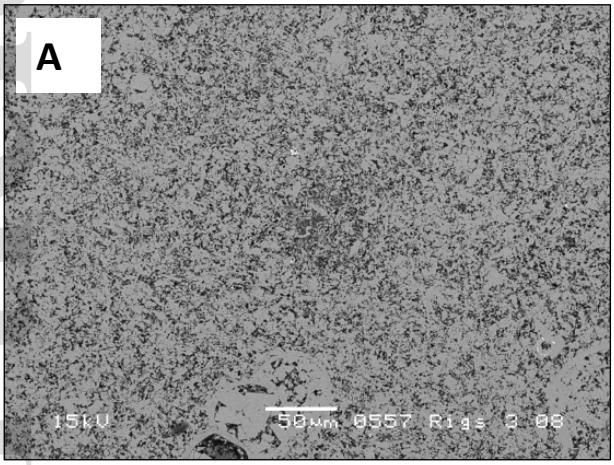

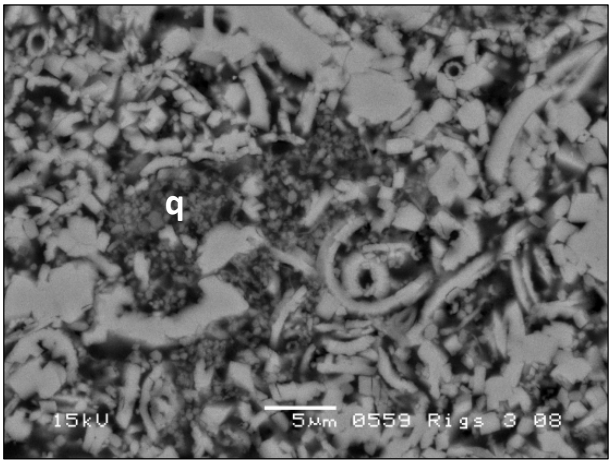

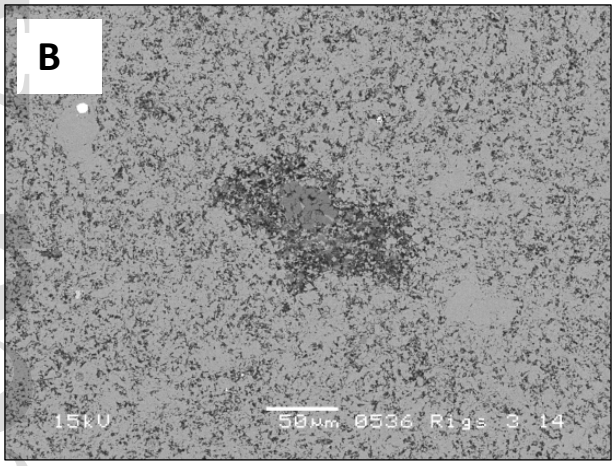

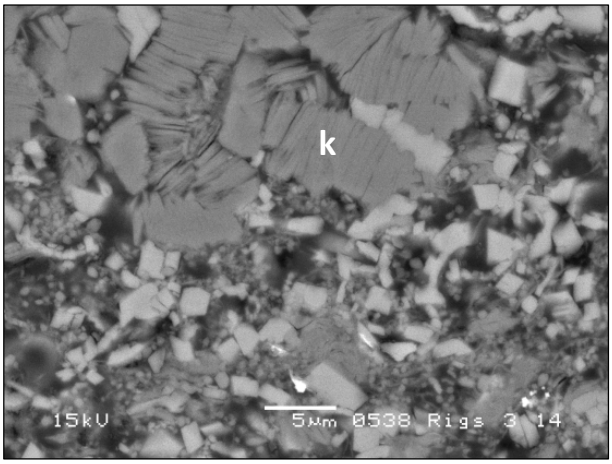

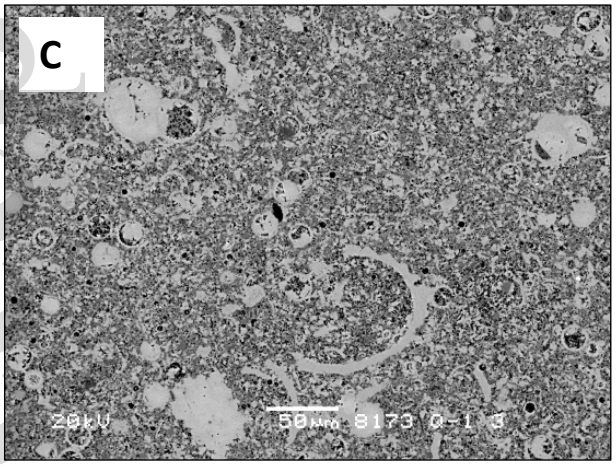

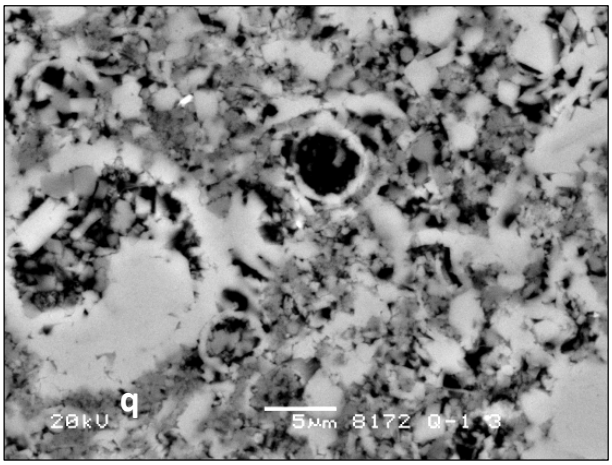

Porosity in chalk - figures

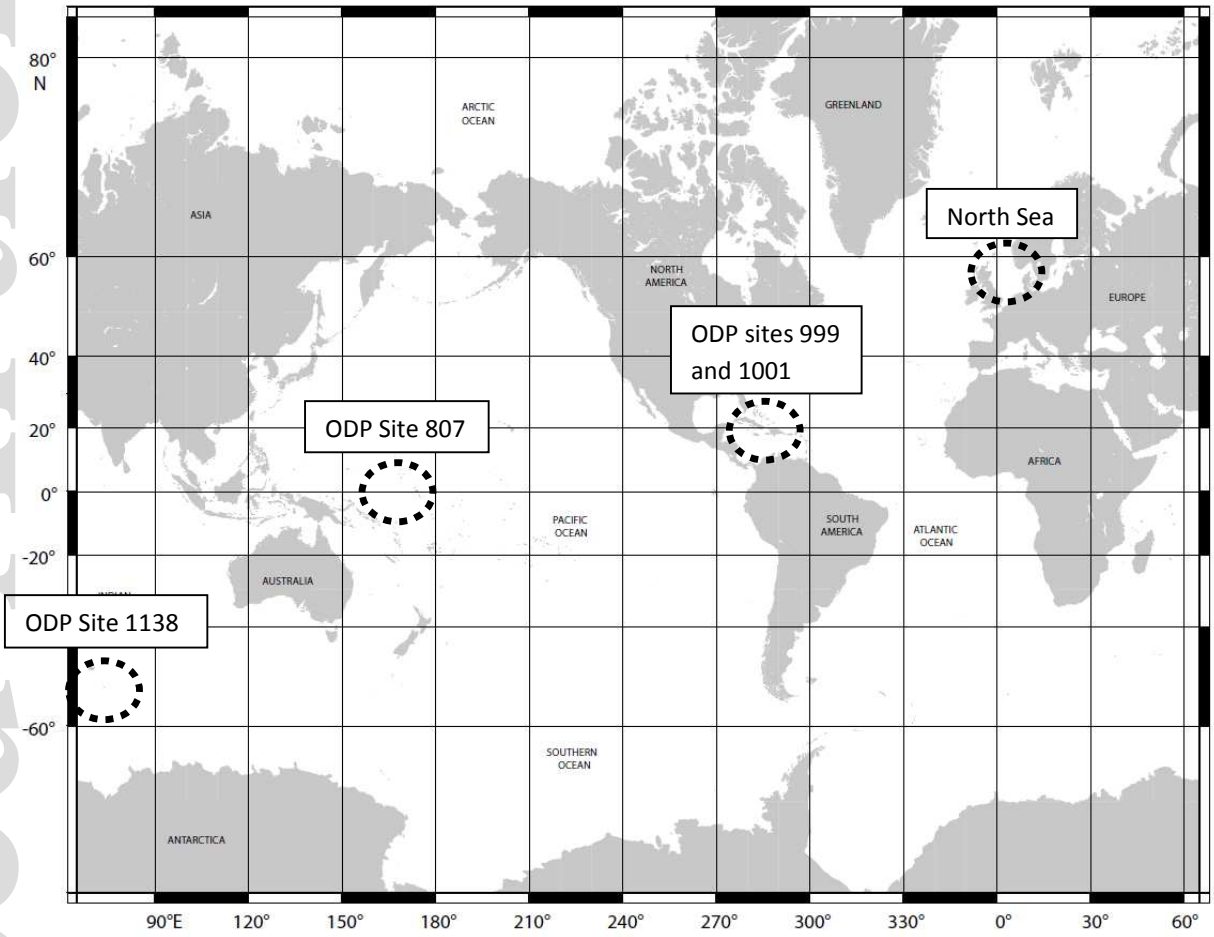

Fig. 5. Locations from where samples were collected (modified after http://www-odp.tamu.edu/sitemap/sitemap.html).

Fig. 6. Stylolite following compaction bands (photo: Ida Lind, Tidsskriftet Varv 1993, 2, front page).

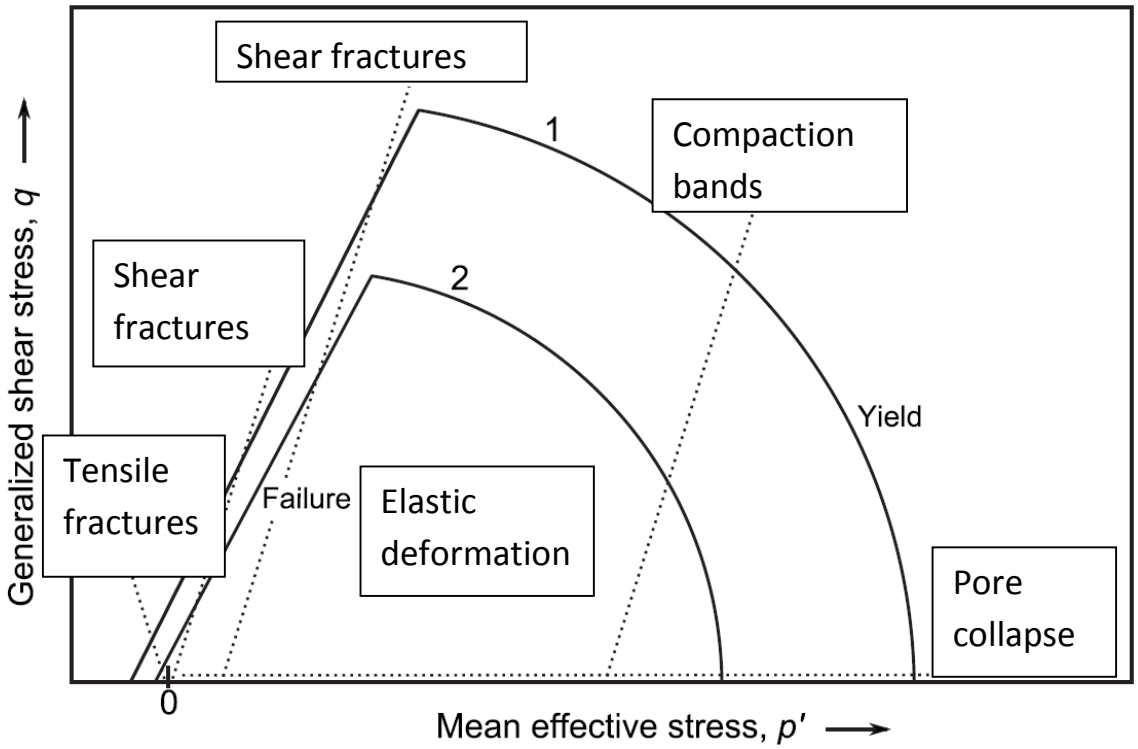

Fig. 7. *p*-*q* diagram displaying area of elastic deformation, limit for failure (formation of fractures: steep solid line) and yield envelope where compaction bands form. Yield under hydrostatic conditions causes pervasive pore collapse. The figure compares the diagram for a strong (1) and a weak (2) sample. The dotted lines show experimental stress paths needed for constructing the diagram. Mean effective stress. $p' = \frac{1}{3}(\sigma_1' + \sigma_2' + \sigma_3')$. Generalized shear stress, $= \frac{1}{\sqrt{2}}\sqrt{(\sigma_1 - \sigma_2)^2 + (\sigma_2 - \sigma_3)^2 + (\sigma_1 - \sigma_3)^2}$, where $\sigma_1, \sigma_2, \sigma_3$ are the three principal stresses (Andreassen & Fabricius, 2010).

Porosity in chalk - figures

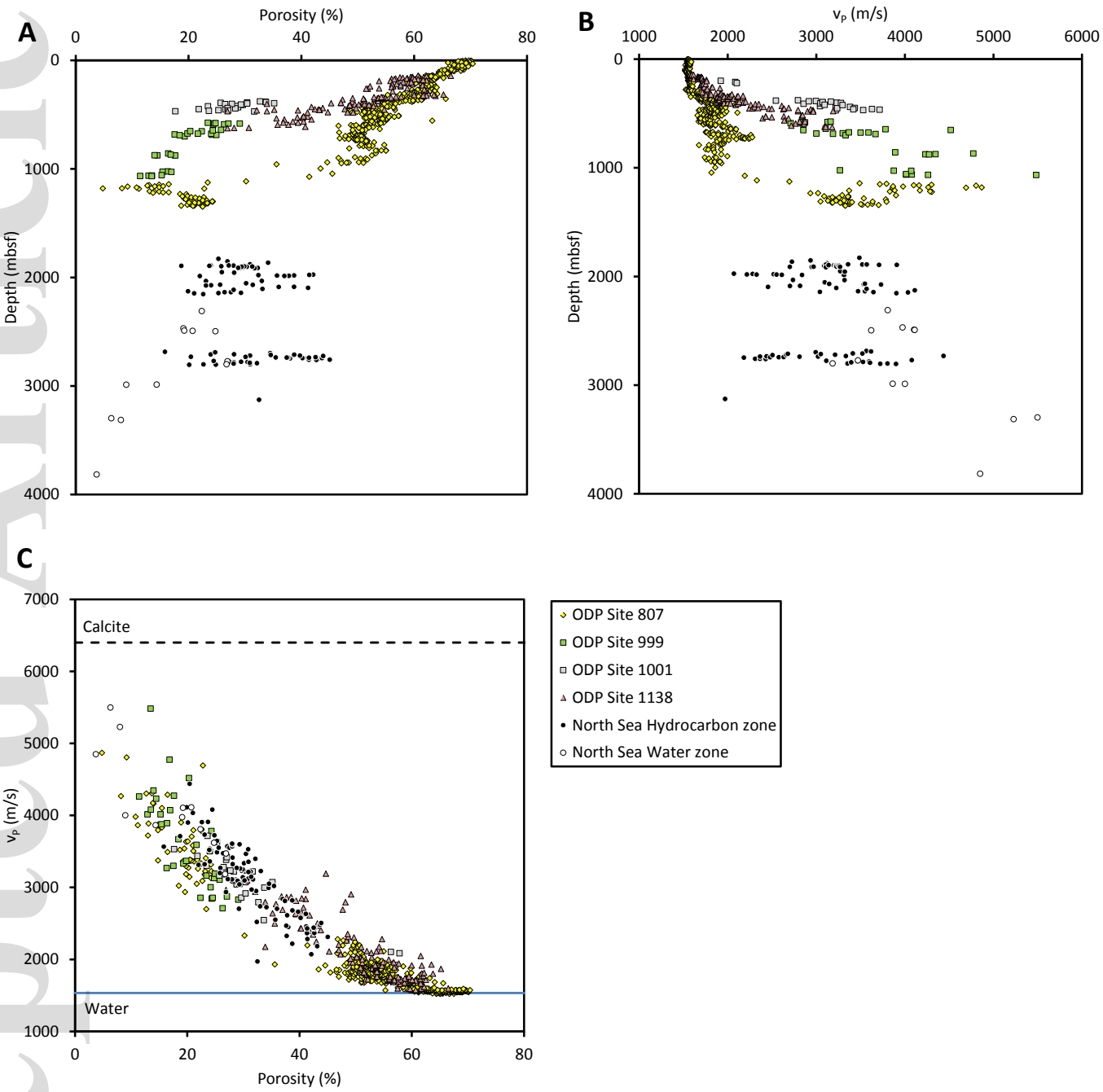

Fig. 8. Cross-plots of raw data for the studied samples annotated with sample location. (A) Porosity vs. depth below sea floor (mbsf). (B) P-wave velocity, V_P, of water saturated samples vs. depth (mbsf). (C) V_P vs. porosity.

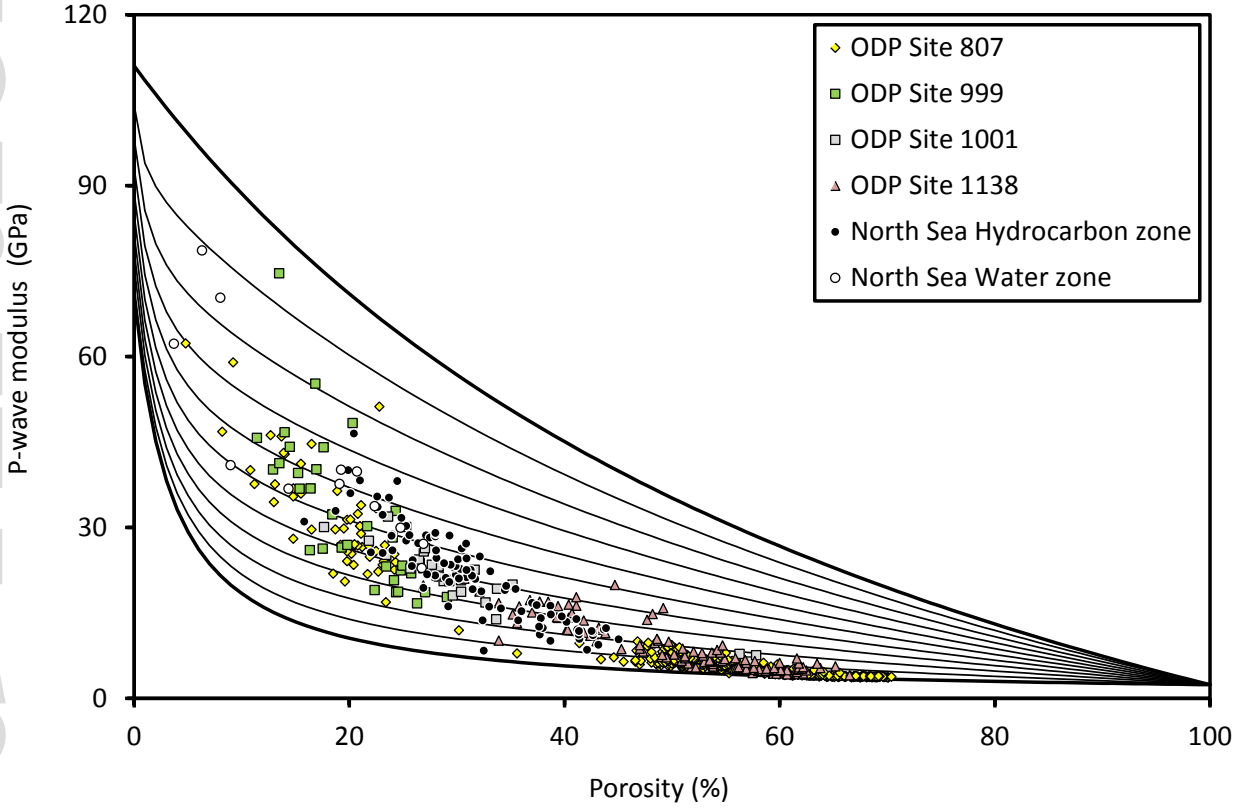

Fig. 9. Cross-plot of P-wave modulus of water saturated samples and porosity. The type curves refer to iso-frame value 0 (lowest) to 1.0 (uppermost).

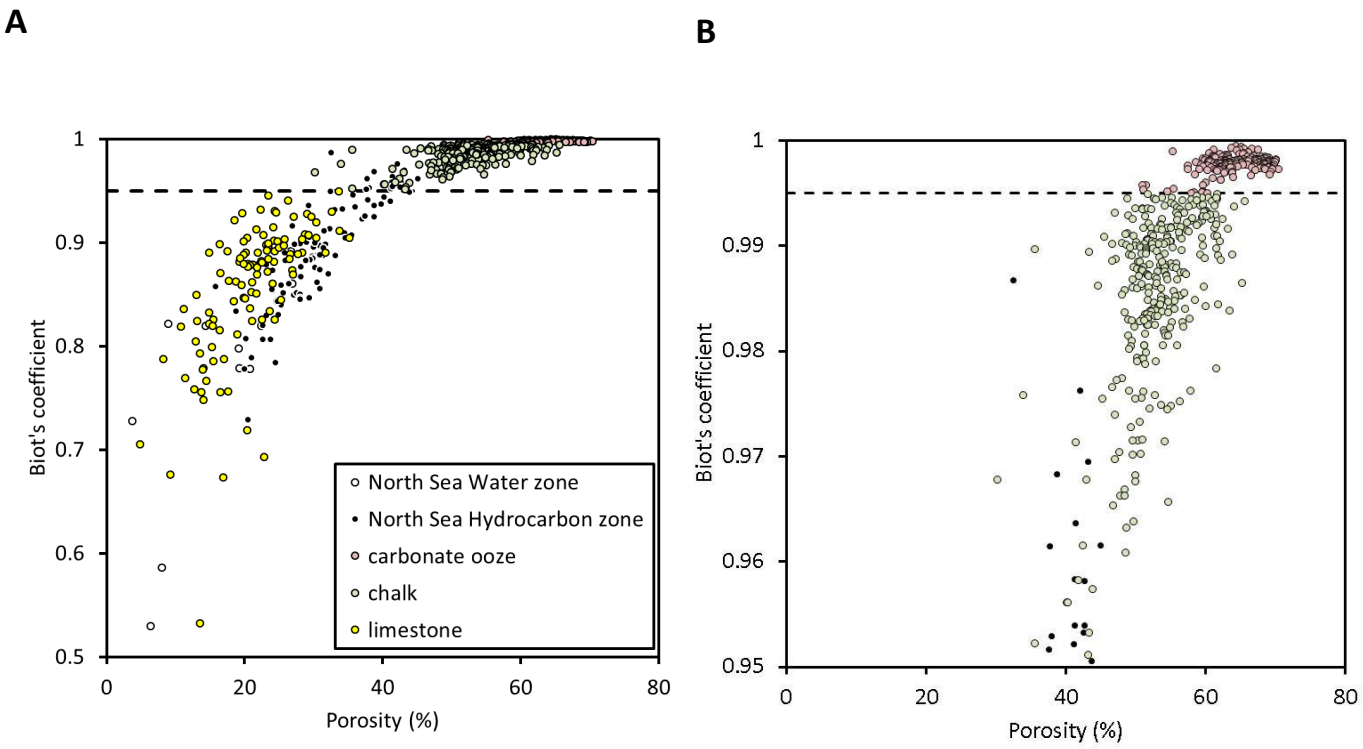

Fig. 10. (A) Cross-plot of Biot's coefficient and porosity. (B) Detail of uppermost part of (A).

Porosity in chalk - figures

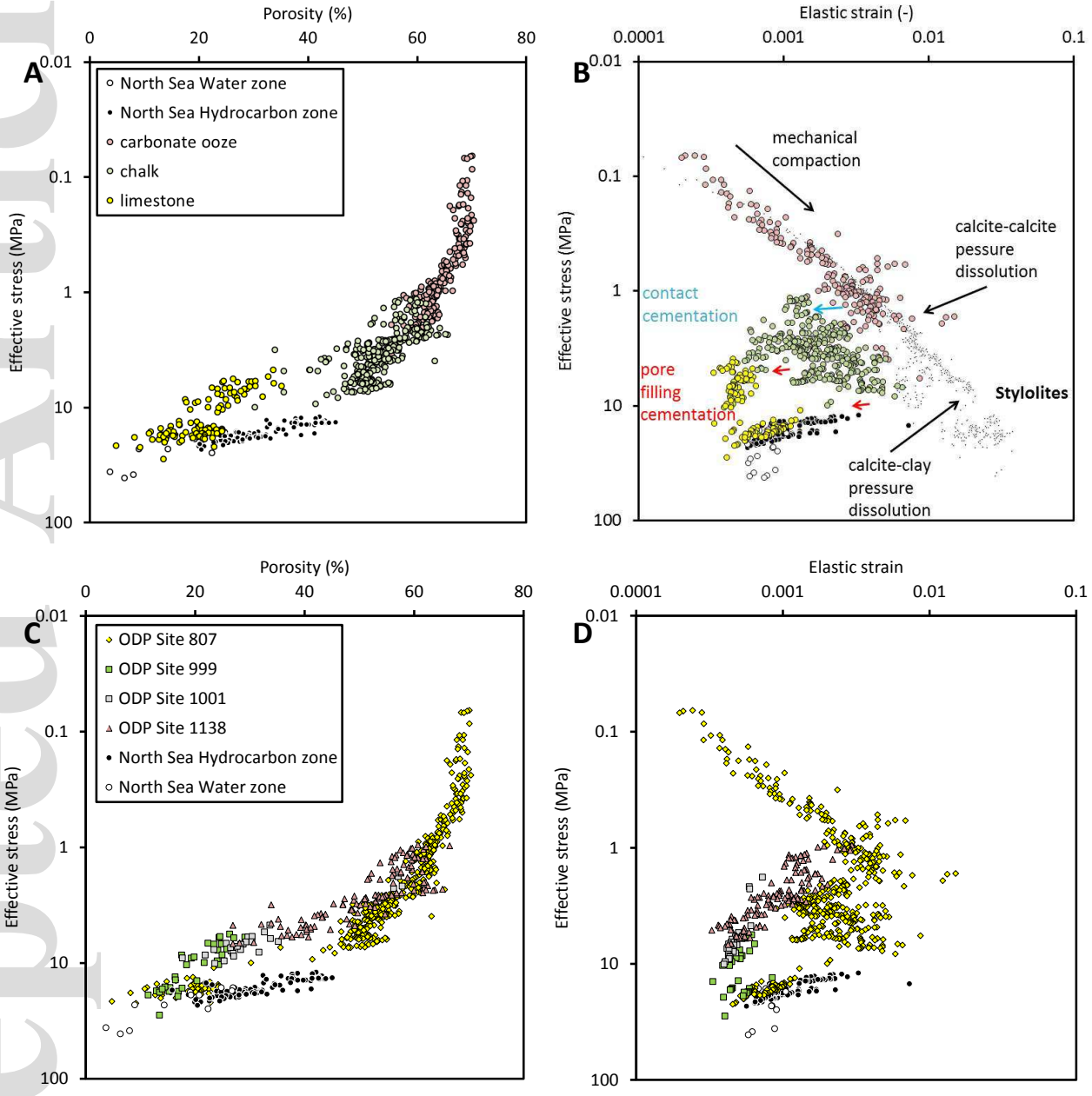

Fig. 11. Cross-plots of porosity (**A**) and (**C**) and elastic strain (**B**) and (**D**) vs. effective stress; annotated with respect to lithology (**A**) and (**B**) and locality (**C**) and (D). (**B**) An interpretation of how effective stress and elastic strain reflect diagenetic processes. Circles represent elastic strain calculated according to Biot (Eq. 2). Tiny dots represent modelled strain at the same samples after a thought pore collapse causing elastic modulus to drop and strain to increase.